Green Fluorescent Protein-based pH indicators for *in vivo* use: a review

RANIERI BIZZARRI,[‡¶]* MICHELA SERRESI,[‡] STEFANO LUIN,[¶] AND FABIO BELTRAM[‡¶]

[‡]*Scuola Normale Superiore – NEST laboratory, Italian Institute of Technology research unit, piazza dei Cavalieri 7, 56126 Pisa, Italy*

[¶]*Scuola Normale Superiore – NEST CNR-INFM, piazza dei Cavalieri 7, 56126 Pisa, Italy*

*Corresponding author: r.bizzarri@sns.it, ph: +39-050-509434, fax: +39-050-509417

Abstract

Green fluorescent protein (GFP) and its variants have been used as fluorescent reporters in a variety of applications for monitoring dynamic processes in cells and organisms, including gene expression, protein localization, and intracellular dynamics. GFP fluorescence is stable, species-independent, and can be monitored non-invasively in living cells by either fluorescence microscopy, flow cytometry or macroscopic imaging techniques. Owing to the presence of a phenol group on the chromophore, most GFP variants display pH-sensitive absorption and fluorescence emission bands. Such a behavior has been exploited to engineer genetically-encodable pH indicators for studies of pH regulation within specific intracellular compartments that cannot be probed using conventional pH-sensitive dyes. These pH indicators contributed to shed light on a number of cell functions for which intracellular pH is an important modulator. In this review we discuss the photophysical properties that make GFPs so special as pH indicators for *in vivo* use and we describe the probes that are more utilized by the scientific community.

1. Introduction

Intracellular pH (pH_i) is a fundamental modulator of cell function [1]. Because of the high reactivity of H^+ ions with proteins, pH_i influences processes as varied as cell metabolism and growth [2, 3], ionic current flow through membrane channels (and hence cellular excitability) and solute movement on membrane transporter proteins (and hence vectorial water movement, and general ion homeostasis) [4, 5] and, in the case of muscle, cellular contractility [6]. pH_i of eukaryotic cells is normally in the range 7.1–7.4, and is regulated by the flux of acid equivalents (H^+, OH^- or HCO_3^-) across the surface membrane, usually on specific ion-coupled transporters such as the NHE proteins [5]. pH_i is also influenced by acid-generating processes, such as aerobic and anaerobic metabolism [7]. The increased H^+ efflux at the leading edge of migrating fibroblasts is necessary for cell polarity, de-novo actin polymerization, and efficient cell movement [8]. NHE exchangers play a critical role in mediating cytoskeletal reorganization by integrin receptors and by the Rho family of GTPases [9]. It is well established that both the activation of NHE1 and increases in pH_i are early and universal responses to mitogens and have permissive effects in promoting cell proliferation [3].

Notably, pH_i is not spatially uniform and depends on the nature and function of subcellular domains. In the endocytic pathway, the progressive luminal acidification of endosomes is essential for the distribution and degradation of internalized ligands into lysosomes [10]. The decreased pH of early endosomes favors dissociation of many incoming receptor-ligand complex. Various combinations of active Na^+/K^+ ATPases and active chloride channels were proposed to explain differences in pH between early, recycling, and late endosomes within many cell types [11].

The synaptic activity is another biological event regioselectively regulated by pH. Neurotransmitters stored in presynaptic vesicles are released through the fusion of vesicles

with the plasmamembrane by a process known as exocytosis [12]. The lumen of presynaptic vesicles displays an acidic interior. During exocytosis the synaptic vesicle fuses with the surface membrane and undergoes a pH jump. After fusion, the inside of the vesicle comes in contact with the extracellular medium with a pH around neutrality.

Alterations in intracellular pH strongly affect cell viability. For instance, mithocondria are characterized by mildly alkaline pH and deviations from this pattern are believed to be essential in the regulation of the so called "permeability transition pore" and thus in controlling apoptosis [13]. The maturation and processing of secretory proteins in vesicular compartments requires acidic pH into the lumen of organelles. The aberrations of the normal organellar pH homeostasis can lead to an impairment of posttranslational modifications and processing of secreted proteins [14], to a mislocalization of the biosynthetic cargo [15], and to severe defects in functionality of the organelles [16]. Alterations of the pH of the secretory pathway often have severe consequences. Abnormalities noted in many human tumors (i.e breast cancer and colorectal cancer) and papillomas have also been attributed to modification of the pH of the secretory compartment [17].

Quantitative fluorescence imaging microscopy has become a powerful tool in cell and molecular biology because it permits the measurement of both spatial and temporal dynamics of molecules and organelles in living cells [18]. The superior sensitivity, specificity, and spectroscopic capabilities of fluorescence microscopy encouraged the development of advanced detection systems, physical optical methods, and fluorescent probes and indicators. Given its relevance for cell biology, the proton concentration has been one of the first *in vivo* parameters to be monitored by fluorescent probes [19, 20]. Nowadays, spatially resolved fluorescence sensing is the only method available for the detection of pH_i with high spatial resolution [18, 21]. This technology greatly benefited of the recent engineering of a set of outstanding fluorescent probes, the **green fluorescent proteins** (GFPs). In this review, we shall discuss the intrinsic properties that tailor GFPs to the detection of pH_i (§ 2-4) and the

advantages of their use over common dyes (§ 4-5). Then, we shall describe the GFPs better suited to *in vivo* pH measurements up to date (§ 6), the typical microimaging setups adopted for these measurements (§ 7), and finally we shall illustrate the application of non-linear microscopy to pH-sensing by GFPs, presenting also some new data of ours (§ 8).

2. Green Fluorescent Proteins: relevance, structure, and chromophore formation

The Green Fluorescent Protein (GFP) was discovered in 1962 as an accessory protein of the bioluminescence system of the hydroid jellyfish *Aequorea Victoria* based on the protein aequorin [22]. The successful purification of the protein and the subsequent spectral characterization showed that it absorbs blue light and emits green light, thus playing the role of converter of aequorin's blue chemoluminescence into the greenish bioluminescence of the jellyfish [23]. Thirty years later the cloning [24], and the successful heterologous expression of the GFP gene [25], provided the clear demonstration that the green fluorescent emission is genetically encoded into the primary sequence of the protein and no jellyfish-specific cofactors are needed for the synthesis of the chromophore. Accordingly, GFP can be used as an intrinsic intracellular reporter of target proteins by simple genetic fusion and subsequent gene transfer and expression into cells.

The rational modification of the wild type GFP primary sequence yielded many mutants with different colors and photophysical properties [26]. Recently, the color palette of GFPs has been expanded by the discovery and engineering of new red-shifted proteins from *Anthozoa* corals [26-28]. The primary advantages of fluorescent protein-based indicators over simple organic dyes are that they can be designed to respond to a much greater variety of biological events and signals, targeted to subcellular compartments, introduced in a wider variety of tissues and organisms, and they seldom cause photodynamic toxicity [29]. In this review we

shall limit our discussion to mutants belonging to the *Aequorea* family (GFPs), on account of the general poor pH-responsiveness and more complex photophysics of red fluorescent proteins from *Anthozoa* and other corals [28].

Wild type GFP (wtGFP) is constituted by a single peptide chain of 238 aminoacids that has a molecular weight around 27 kDa.[23] As highlighted by X-ray spectroscopy, this sequence folds in a compact cylindrical three-dimensional structure with a diameter of 24 Å and a height of 42 Å (Figure 1) [30]. Such a cylindrical structure, often referred to as β-can or β-barrel, stems from the ordered arrangement of 11-stranded β-sheets. The β-barrel is capped on both ends by short α-helical sections and run through by a α-helix, which contains the three aminoacids forming the chromophore.

The chromophore of GFP is buried at the center of the β-barrel (Fig. 1), and originates from the spontaneous post-translational cyclization of three consecutive aminoacids: Ser^{65}-Tyr^{66}-Gly^{67} following the formation of the native β-barrel tertiary structure. This topic was recently reviewed by Wachter et al. [31]. The correct folding and configuration of the residues around the chromophore are pre-requisites for fluorescence, as the isolated chromophore is not fluorescent in aqueous solution [32]. Indeed, the presence of the compact and rigid tertiary structure of GFP is thought to be responsible for the high quantum yield of fluorescence emission [33]. Owing to the chromophore-enveloping tertiary structure, many of the classical fluorescence quenching agents are almost ineffective on GFP emission, and denaturation occurs only above 76 °C [34].

Notably, inside the protein the chromophore is surrounded by four entrapped water molecules and a surprising number of charged and polar residues, among which Gln^{69}, Gln^{94}, Arg^{96}, His^{148}, Thr^{203}, Ser^{205}, and Glu^{222} [35]. These residues provide several proton donor and acceptor groups that participate in a structured hydrogen-bond network responsible of the

spectral and photophysical properties of the protein [35-37]. Arg^{96} and Glu^{222} are known to play a relevant role also during the chromophore formation [38].

3. Protonation reactions of the GFP chromophore: the basis of pH sensing

Photophysical characteristics of the neutral and anionic GFP chromophore

In principle, four protonation states (Scheme 1, **I-IV**) are accessible to the GFP chromophore, owing to the acid-base properties of both the phenol group on the Tyr^{66} aromatic ring and the N^{66} (pdb nomenclature, ref. [39]) nitrogen on the imidazolinone ring. In the isolated chromophore, N^{66} has a pK = 1.8-2.4 (**III↔I**) whereas the phenol group has pK=8.1-8.5 (**I↔II**) [40, 41]; additionally, the phenol group was found to have a pK=6.5 when N^{66} is in a quaternary positively-charged state similar to the protonated one (**III↔IV**) [41]. From these pK values it is easy to calculate that less than 0.01% of the overall chromophore in the neutral state must be present as zwitterion (**IV**). Thus, above pH 3, only the proton exchange reaction of the phenol group is relevant to determine the ground state of the chromophore (**I↔II**), and no protonation pathways leading to the fully protonated (**III**) or zwitterionic (**IV**) states are truly active. This situation holds also in the folded protein [42], although the deprotonation of the phenol group takes place at a significantly lower pH value (pK=5.2-7.5) [37, 42-44]. Forms **I** and **II** (Scheme 1) are traditionally called state A and B, respectively.

The optical properties of A and B states are considerably different in GFPs. In wtGFP, state A absorbs at 398 nm and emits at 508 nm, whereas state B absorbs at 475 nm and emits at 503 nm [23]. The actual absorption wavelengths change in other variants, but the spectral pattern remains the same: state B absorbs at a much longer wavelength than state A (up to 100-120 nm), whereas their fluorescence emissions display a considerable degree of resemblance. These absorption properties were easily explained in terms of an extended electronic

conjugation in the B phenol-anionic state, which lowers the $S_0 \rightarrow S_1$ transition energy [45]. The mechanism at basis of the fluorescence similarity is subtler and was elucidated only by means of fast spectroscopic methods [46]. Indeed, A and B states differ not only in the protonation of Tyr^{66}, but also for the dissimilar conformation of the residues surrounding the chromophore [35]. According to available x-ray structures of wtGFP and other variants, a peculiar hydrogen-bond network connecting the phenol group to residue Glu^{222} is present in A state, whereas it is interrupted in B state. When GFP is excited in the anionic B state, it emits directly from the excited state B*. Conversely, when the A state is excited, two fluorescence emission channels are active: i) direct emission from A* state and ii) deprotonation of A*, owing to the much increased acidity compared to the ground state [45], with a concomitant proton transfer to Glu^{222} [46, 47]. The latter mechanism is called *Excited State Proton Transfer* (ESPT) and occurs in few picoseconds, usually overwhelming the direct A* weak emission that occurs in the 440-460 nm region [48]. ESPT leads to an intermediate excited form, usually denoted by I*, which is characterized by a deprotonated chromophore similar to B*; hence, I* resembles B* for the emission energy [49]. The slight difference between B* and I* emissions arise only from environmental effects, as the short timescale of A*→I* process does not allow the rearrangement of the residues surrounding the chromophore (e.g.: Thr^{203}) to the relaxed configuration typical of the anionic state [46, 49]. Deactivation of I* leads to I, a metastable ground-state species characterized by the anionic chromophore embedded in an environment typical of its neutral form. The I moiety eventually evolves to the A state, which is about 7.6 kJ/mol lower in energy [50], by receiving back the proton of Glu^{222} through an internal protonation relay involving Ser^{205} and a bound water molecule [35]. Careful kinetic analysis of the full Förster cycle related to A emission revealed that the I species actually comprises two metastable intermediates I_1 and I_2, although I_1 is very short lived (3 ps) compared to I_2 (0.4 ns) [51]. The same kinetic study showed that I_1 and I_2 have a red-shifted absorption compared to B in wt-GFP ($I_{1\text{-}2}$: 497-500 nm). Interestingly, these data

are in excellent agreement with those reported for a GFP variant that contains sequence mutations specifically designed to stabilize the I state of the chromophore [50].

In wt-GFP the equilibrium between the A and B states is affected by a number of factors such as temperature, ionic strength, protein concentration, and, in a peculiar way, pH. Indeed, wt-GFP shows pH-dependent absorption/fluorescence spectra at pH around 4.5-5 and 9-10, with impressive absorption/emission stability in the physiological pH range. This behavior is a consequence of molecular optimization of wt-GFP by natural selection to play a functional role in in *Aequorea Victoria* jellyfish. Remarkably, also the fluorescent protein recovered from coral organisms display almost no change in emission in the physiological pH range [28, 52]. Engineered GFP mutants, however, have no natural role to play and in many cases were found to possess a fast equilibrium (< ms [53, 54]) between the neutral and anionic form of the chromophore in the 5-8 pH interval. Additionally, GFP mutants devoid of Thr^{203} usually do not display structural relaxation upon chromophore protonation/deprotonation. Hence, only if the ESPT from A* leads to a chromophore environment slightly different in terms of polarity/electronic density from that of B*, is the distinction between I* and B* still meaningful.

In the following, we shall consider the effect of pH on the simple ground-state A↔B equilibrium, implicitly assuming that structurally/environmentally "non-relaxed" anionic species I (if present) negligibly contribute to the protein absorption spectra on account of their metastable character and short lifetime. Nonetheless, we shall highlight whether the emission from A state involves an ESPT mechanism or not, and if there are differences between the ESPT-based emission and that of B* (indicating the presence of an I* moiety).

Fluorescence dependence upon pH

The difference in optical characteristics between states A and B is at basis of the use of GFP variants as pH indicators [53]. Indeed, A and B interconvert into each other as pH is varied,

thus generating a series of absorption and fluorescence spectra (Fig. 2a). This photophysical behavior is amenable to simple mathematical description, if: 1) each state maintains its optical characteristics when the pH is varied, and 2) a linear relationship holds between fluorescence and concentration (typical of diluted solutions). Let K be the generic equilibrium constant of the ionization of the phenol group (Scheme 3), the concentrations of the A and B states can be calculated from the mass action law as:

$$[A] = C_0 \cdot \frac{10^{(pK-pH)}}{1+10^{(pK-pH)}} \qquad [1]$$

$$[B] = C_0 \cdot \frac{1}{1+10^{(pK-pH)}} \qquad [2]$$

where C_0 is the overall concentration of the protein. According to our previous hypotheses, the fluorescence excited at λ_x and emitted at λ_e will depend pH as:

$$F(\lambda_x,\lambda_e) = C_0 \cdot \left(\frac{F_B(\lambda_x,\lambda_e) + F_A(\lambda_x,\lambda_e) \cdot 10^{(pK-pH)}}{1+10^{(pK-pH)}} \right) \qquad [3]$$

where $F_A(\lambda_x,\lambda_e)$ and $F_B(\lambda_x,\lambda_e)$ are the molar fluorescence emissions of the A and B states, respectively. $F_A(\lambda_x,\lambda_e)$ and $F_B(\lambda_x,\lambda_e)$ account for both the extinction coefficient and quantum yield of the protein as well as the light source intensity and collection efficiency of the spectroscopic/imaging apparatus. For most mutants $F_B(\lambda_x,\lambda_e) > F_A(\lambda_x,\lambda_e)$ in a wide interval of wavelengths (this trend being reversed only in proximity of the absorption maximum of A) owing to the larger brightness (the product of extinction coefficient and quantum yield) of B compared to A. Equation 3 indicates that the protein fluorescence retains sigmoidal

dependence on pH (Fig. 2b), in agreement with the typical isotherm for a single-proton dissociation. At pH=pK, the fluorescent signal reaches half of its overall variation [$F_B(\lambda_x,\lambda_e)$-$F_A(\lambda_x,\lambda_e)$]. Differentiation of Eq. 3 shows also that the maximum signal sensitivity to pH changes is found in the pH range [pK-1;pK+1], where the fluorescence response to pH is nearly linear (maximum deviation: 16%).

Two-site (2S) model of chromophore protonation in GFPs

Most components of the GFP family (possessing the phenol group of Tyr^{66}) follow the pH pattern of fluorescence described by Eq. 3. Some variants, however, are characterized by spectral features that are not compatible with the simple scheme of phenol ionization, though the pH dependence of emission still complies with Eq. 3. For instance, in these mutants the absorption of the neutral chromophore is still detectable at pH values where the fluorescence has reached its upper asymptote [43, 55]. To rationalize the pH-dependent optical behavior of all GFPs, we proposed a comprehensive protonation model considering both the chromophore and an environmentally close second protonation site X (2S model, Scheme 3) [43]. The 2S model entails four distinct ground states (A', A, B, and B'), which correspond to the four possible combinations of protonation state of the chromophore/X couple. According to the 2S model, the X site affects the optical characteristics of the protein only if it is *thermodynamically coupled* to the ionization of the chromophore (the protonation state of X modulates the chromophore's pK and vice-versa) [56]. If uncoupled, the X site plays a role in determining the kinetics of the proton exchange between the chromophore and the external buffer [43, 54], but the optical properties of the protein follows the simple equilibrium of Scheme 2. Inspection of the GFP structure shows that only two residues are close enough to the chromophore and ionizable in the stability range of the protein: His^{148} and Glu^{222}. We found that the GFP variants for which X and the chromophore are uncoupled are characterized by X=His^{148} [43]. Remarkably, when X= Glu^{222}, X and the chromophore were

found to be so strongly anti-cooperatively coupled (i.e. deprotonation of one forbids the deprotonation of the other) that the fully deprotonated state B' could not be reached within the stability pH range of the protein. In such a case it was shown theoretically that the optical response of the protein follows the *single ionization* of the fully protonated A' state to an apparent mixed form of A and B states [43]. This effect explains, for instance, why the absorption spectrum at high pH state retains features of the neutral chromophore.

The ionization coupling between Glu^{222} and the chromophore can be understood by considering the presence of two closely spaced negative charges in the B' state, i.e. the anionic Glu^{222} and the anionic chromophore. Owing to electrostatic repulsion between these two charges poor thermodynamic stability is expected in this configuration. The lack of significant coupling between His^{148} and the chromophore is less intuitive. Here, the A' and B' states are characterized by only one net charge (positive in A' and negative in B'), but the presence of a positive or neutral charge on His^{148} seems not to influence the ionization of the chromophore. We believe that the shielding of the positive charge on His^{148} (A' and B states) can be ascribed to an H-bonding interaction with the backbone oxygen of the spatially close Asn^{146}, as reported for the S65T mutant at rather low pH [42].

So far the 2S model has been successful in explaining the pH-related optical properties of all GFP variants we examined. Thermodynamic coupling arises whenever the Glu^{222} residue is not forced into a single protonation state by the H-bonding action of nearby residues, like Thr^{65} in S65T GFP [42]. Nonetheless, both "coupled" or "uncoupled" mutants display analogous pH dependence of the optical response, described by Eq. 3. Thus, all GFP mutants with Tyr^{66} are in principle utilizable as pH indicators *in vivo*, provided that their pK values fall in the pH range of the envisaged application. Some "coupled" variants (among which stands wtGFP), however, are characterized by a powerful buffering effect of the Glu^{222} residue on chromophore ionization, resulting in a substantial independence of the optical

response from pH in the physiological range. Therefore these mutants are unsuitable for pH sensing *in vivo*.

4. Ratiometric fluorescent indicators

Eq. 3 shows that the emission intensity of a pH indicator depends on the total concentration of the protein C_0. Therefore, it is difficult to determine whether observed changes in fluorescence are due to pH changes or indicator GFP concentration. In living specimens, it is nearly impossible to control protein expression in the same way in several cells at the same time. Additionally, if the imaging system is not confocal, the fluorescence response of the indicator will be affected by cell thickness, as the probe excitation is proportional to the length of the optical path. A remarkable way to circumvent these problems is represented by **ratiometric GFP pH indicators**, which do not require an independent means of measuring concentration of the probe. The theoretical analysis of ratiometric pH indicators, in a form equivalent to that developed by Grynkiewicz for Ca^{2+}-sensors [57], is presented in the following.

Let us consider a GFP mutant whose fluorescence obeys Eq.3 and two sets of excitation-emission wavelengths or wavelength intervals (λ_{x1},λ_{e1}) and (λ_{x2},λ_{e2}). If we take the ratio of fluorescence in these two sets we have:

$$\frac{F(\lambda_{x1},\lambda_{e1})}{F(\lambda_{x2},\lambda_{e2})} = \left(\frac{F_{\infty}(\lambda_{x1},\lambda_{e1}) + F_0(\lambda_{x1},\lambda_{e1}) \cdot 10^{(pK-pH)}}{F_{\infty}(\lambda_{x2},\lambda_{e2}) + F_0(\lambda_{x2},\lambda_{e2}) \cdot 10^{(pK-pH)}} \right) \quad [4]$$

where the notation F_A and F_B of Eq. 3 has been replaced by F_0 (lower molar fluorescence asymptote) and F_∞ (higher molar fluorescence asymptote), in keeping with the more general scheme of the 2S model (§ 3). Equation 4 can be recast in a more compact form as:

$$R[1,2] = R_0[1,2] \cdot \left(\frac{R_f[1,2] + 10^{(pK' - pH)}}{1 + 10^{(pK' - pH)}} \right) \quad [5]$$

where

$$R[1,2] = \frac{F(\lambda_{x1}, \lambda_{e1})}{F(\lambda_{x2}, \lambda_{e2})} \quad [6]$$

$$R_0 = \frac{F_0(\lambda_{x1}, \lambda_{e1})}{F_0(\lambda_{x2}, \lambda_{e2})} \quad [7]$$

$$R_f = \frac{F_\infty(\lambda_{x1}, \lambda_{e1})}{F_0(\lambda_{x1}, \lambda_{e1})} \cdot \frac{F_0(\lambda_{x2}, \lambda_{e2})}{F_\infty(\lambda_{x2}, \lambda_{e2})} \quad [8]$$

$$pK' = pK - \log\left[\frac{F_\infty(\lambda_{x2}, \lambda_{e2})}{F_0(\lambda_{x2}, \lambda_{e2})} \right] \quad [9]$$

R[1,2] is called the *ratiometric fluorescence signal* of sets #1 and #2. Most frequently ratiometric indicators work either *by excitation* ($\lambda_{x1} \neq \lambda_{x2}$, $\lambda_{e1} = \lambda_{e2}$) or *by emission* ($\lambda_{x1} = \lambda_{x2}$, $\lambda_{e1} \neq \lambda_{e2}$).

It is worth noting that Eq.5 and Eq. 3 have the same functional dependence upon pH. Thus, a plot of R[1,2] *vs* pH would show a sigmoidal shape whose lower asymptote is represented by R_0 (the *ratiometric offset*), the amplitude by R_f (the *dynamic range*), and the mid-point by pK' (the *ratiometric pK*) (Fig. 3). Differently from Eq. 3, however, Eq. 5 does not retain the

dependence from the protein concentration C_0 found in Eq. 4, and has therefore general validity in the system under observation. Furthermore, the ratiometric nature of all parameters makes R[1,2] independent from geometrical features, such as cell or specimen thickness, as well as from general fluorescence variations due to photobleaching effects. Accordingly, it is often said that Eq. 5 describes a *general or universal calibration curve* under the selected excitation/observation conditions.

From Eq. 7, we see that R_0 is influenced by instrumental characteristics such as the excitation intensity and the detector efficiency, as it represents a fluorescence ratio taken adopting two specific excitation/emission optical sets. Instead, Eqs 8-9 show that R_f and pK' depend only on the photophysical/thermodynamic properties of the fluorescent protein and on the selection of the excitation/emission sets (λ_{x1},λ_{e1}) and (λ_{x2},λ_{e2}). The nature of set (λ_{x2},λ_{e2}) is particularly relevant, as it contributes to defining pK', the mid-point of fluorescence response upon pH (Eq. 9). Thus, careful selection of this set is required to tailor the pH indicator to the desired biological application(s), as maximum sensitivity of ratiometric signal to pH occurs in the range [pK'-1;pK+1], where R[1,2] *vs* pH is nearly linear. A special case occurs when $R_f = 1$, i.e. the same optical variation upon pH is experienced by the fluorescent probe in the (λ_{x1},λ_{e1}) and (λ_{x2},λ_{e2}) sets. In such a case the ratiometric measurement is not feasible (R[1,2] is always constant). Therefore, only those fluorescent probes characterized by multiple excitation or emission maxima that show opposing changes in fluorescence excitation or emission in response to pH are utilizable as ratiometric pH indicators.

GFP mutants ideally stand as excellent ratiometric indicators by excitation, owing to the large absorption and excitation difference between the neutral and anionic chromophore. Nonetheless, most pH sensitive GFP mutants display pK values at margins of the physiological range and/or poor emissivity of the neutral chromophore, and cannot be employed to monitor ratiometrically pH *in vivo*. We will discuss the most relevant GFP-based

ratiometric pH indicators by excitation in § 6, showing also that few GFP variants (for which the emission is significantly altered upon pH changes) are good candidate to report ratiometrically pH changes *in vivo* by emission.

5. Spatial resolution of GFP-based pH indicators

As stated in §1, pH_i is never constant throughout the cellular body, as many biochemical mechanisms are responsible for the presence of different pH values at different locations. A good pH indicator must be capable of reporting a close estimate of the actual pH in every sub-cellular region it comes in, i.e. to provide a realistic pH_i map. Equation 5 provides the general calibration curve that allows to associate each R[1,2] value to a definite pH. Equation 5, however, describes the mathematical linkage between R[1,2] and pH at *thermodynamic equilibrium*. Nothing is said about the *characteristic time* (τ_c) required to reach the equilibrium state. This value is particularly relevant as the fluorescent indicator undergoes another kinetic process while monitoring pH: *translational diffusion*. If the diffusion is much faster than the kinetic relaxation to equilibrium, then measurement of pH_i could be biased, unless the pH_i is rather homogeneous. In the following we shall treat analytically this effect. For simplicity let us consider the equilibrium between CroH and Cro, indicating the neutral and anionic chromophore, respectively. From relaxation analysis, we have that τ_c is linked to the kinetic parameters of the CroH/Cro proton exchange according to:

$$\frac{1}{\tau_c} = k_{on}\left([\mathrm{Cro}]_{eq} + [\mathrm{H}^+]_{eq}\right) + k_{off} \qquad [10]$$

where $[Cro]_{eq}$ and $[H^+]_{eq}$ are the concentrations of Cro and H^+ at equilibrium, and k_{on}, k_{off} are the protonation and deprotonation rate constants, respectively ($K=k_{off}/k_{on}$). Thus, the larger are the rate constants and/or the anionic chromophore concentration, the lower is τ_c. Now, in a

time τ_c we may consider that a freely diffusing molecule would travel a linear distance Δw described by [58]:

$$\Delta w = \sqrt{4\mathrm{D}\,\tau_c} \quad [11]$$

where D is the diffusion constant of the molecule. Therefore, Δw will represent the minimum distance between two space points whose pH values can be truly distinguished, i.e. the resolution of the pH measurement. We will name it *kinetic resolution*. As expected, Eq. 11 shows that increasing the diffusion rate of the probe (measured by D) leads to a larger Δw value. In this perspective, pH sensors based on fluorescent proteins (D≈0.1-20 $\mu m^2/s$ [59-61]) prove much more advantageous compared to simple organic indicators (D≈100-300 $\mu m^2/s$ [59]). Assuming the maximum D found intracellularly for a GFP (20 $\mu m^2/s$), corresponding to a freely diffusing single GFP molecule in cell cytoplasm [61], we have $\Delta w \approx 9\cdot(\tau_c)^{0.5}$ μm. Kinetic characterization of a large set of GFP mutants have shown that τ_c is nearly 1-1.5 ms at maximum for concentrations similar to those found *in vivo* [43, 54]; in such an unfavorable case we have $\Delta w \approx 0.29$ μm. As fluorescence pH measurements *in vivo* are usually carried out by a confocal microscope, it is interesting to compare Δw with the spatial resolution of such a system, calculable approximately from Abbe's equation [62]:

$$\Delta d = \frac{\lambda}{2\mathrm{NA}} \quad [12]$$

where λ is the excitation wavelength and NA the numeric aperture of the objective. Considering NA=1.25 and λ=488 nm (typical imaging conditions of green mutants) we have: $\Delta d \approx 200$ nm, a value quite close to the kinetic resolution. Thus, the fast protonation kinetic and the rather slow diffusion of GFP mutants allow for high-resolution pH monitoring *in vivo*. Nonetheless, if the indicator diffusion is slowed or constrained, for instance by fusion with a protein moiety capable to bind to other species in selected intracellular zones, the kinetic

resolution can even improve. For instance, slowly diffusing GFP constructs (D≈ 0.1-5 $\mu m^2/s$) display kinetic resolution well below the optical resolution.

Our simple calculation is further supported by Fluorescence Correlation Spectroscopy (FCS) studies on pH-sensitive GFP mutants, which showed that in the 5-8 pH range the timescale of GFP diffusion across the focal volume is typically slower than the overall kinetics of protonation/deprotonation (note that two-site protonation schemes must be applied to fit the experimental data, consistently with the 2S model) [63-65]. For comparison, pH-dependent organic probes display protonation kinetics faster than diffusion only up to pH 6 [65, 66]. It is worth noting that FCS studies are usually carried out with 0.1-10 nM concentrations of fluorescent species: typical cell protein concentrations in the 0.1-10 µM range must lead to faster protonation kinetics (Eq. 10).

6. GFP-based pH indicators applied *in vivo*

The first GFP mutant to monitor the intracellular pH was introduced ten years ago by Alan Verkman and its group [53]. Since then, many GFP variants were engineered and proposed to the attention of the scientific community as genetically-encodable pH indicators for *in vivo* use. Actually, some of these probes provided new insights into subtle biochemical processes for which the proton concentration has great relevance. The developed GFP-based pH indicators can be classified into two general families: non-ratiometric and ratiometric. In the following, we shall review the most efficient indicators in each of these two families.

Non ratiometric pH indicators

This family comprises a large number of GFP mutants that display good pH-responsiveness but are characterized by poor emission from the neutral chromophore, and are therefore unsuitable for ratiometric measurements. Owing to the absence of a general calibration curve

(§ 5), these indicators have been used mostly to report *pH_i changes* rather than pH_i. Verkman and coworkers introduced in 1998 the F65L/S65T GFP variant (called enhanced GFP or EGFP) as sensitive pH indicator [53]. EGFP is characterized by high emissivity of the anionic state in the green (ε_{488}= 60000 $M^{-1}\cdot cm^{-1}$, Φ=0.7, λ_e=509 nm, ref. [43]), although its pK (5.8) makes it not suitable to monitor subcellular components at rather high pH (e.g. mitochondria). Nonetheless, EGFP has been used to monitor pH variations in the cell cytoplasm [53], in the Golgi apparatus [53], and in synaptic vesicle cycling at nerve terminals [67]. Recently, EGFP has been proposed as an effective intracellular pH indicator by using Fluorescence Lifetime Imaging [68].

Several round of mutagenesis generated two pH-sensitive GFPs, called 'Ecliptic' and 'Superecliptic' pHlourins (EcGFP and sEcGFP), which were demonstrated to be better green-emitting pH indicators *in vivo* compared to EGFP [67, 69]. Indeed, these two variants display pK=7.1-7.2 [67], and are therefore more suitable to report on pH_i changes. Additionally, EcGFP and sEcGFP display almost no fluorescence of the neutral chromophore, allowing for the sensitive detection of biological processes associated with pH increase. For instance, these mutants were used to investigate the dynamics of presynaptic secretory vesicles exocytosis down to single event resolution, on account of the fluorescence boost occurring upon synaptic vesicle fusion to the plasma membrane and exposure of the lumen, previously acidic, to the neutral extracellular pH [67, 69]. Actually, EcGFP and sEcGFP have been proposed as general markers of cell exocytosis [68]. In spite of their broad use, no extensive photophysical characterization of these two proteins has been reported, although Fluorescence Correlation Spectroscopy (FCS) experiments supported the existence of a second protonation site near the chromophore in EcGFP, in agreement with the 2S model (§ 4) [70].

S65G/S72A/T203Y GFP (EYFP) is an interesting pH responsive variant that has a red-shifted absorption and emission of the anionic chromophore with respect to conventional GFPs [71]. The neutral chromophore of EYFP is almost unemissive. On account of its pK=7.1, EYFP

was shown to be suitable for cytosolic, Golgi, and mitochondrial matrix measurements by Roger Tsien and coworkers [44]. The yellowish fluorescence and very high emissivity of the anionic chromophore (ε_{514}= 84000 $M^{-1}\cdot cm^{-1}$, Φ=0.61, λ_e=527 nm, ref. [72]) makes EYFP a good selection for multicolor experiments in tandem with pH-unresponsive cyan or green mutants. Unfortunately, EYFP fluorescence is severely quenched by chloride [37, 73], a species fairly abundant in some cell types and subcellular organelles. Attempts at reducing the chloride-sensitivity of EYFP by introducing mutations in the chloride-binding pocket afforded mutants with rather low pK unsuitable for pH monitoring *in vivo* [74].

Ratiometric pH indicators

In spite of their relevance, so far only few truly ratiometric pH indicators based on GFPs have been reported. The first, and probably the most popular one, was described in 1998 by James Rothman and coworkers in the same study that introduced EcGFP [69]. They found that a S202H GFP variant, named Ratiometric pHlourin (RaGFP), displayed a strong increase of the 475 nm excitation band concomitantly with a decrease of the 395 excitation upon pH shift from 7.5 to 5.5. This bizarre photophysical behavior, i.e. the decrease of the anionic chromophore band upon pH rise, has not been elucidated yet. Likely, the proximity [30] of protonatable His^{202} to the chromophore in GFPs determines a strong modification of the protonation pathways affecting the optical response of the protein. RaGFP was used as ratiometric indicator by excitation to measure dynamically the pH of various intracellular compartments, such as the cytoplasm [75], peroxisomes [76], endosomes and the *trans*-Golgi network [77], and the presynaptic secretory vesicles [69]. Typically, RaGFP has been imaged by taking the ratio of fluorescence emitted in the 500-550 nm interval by excitation at 410 and 470 nm [75, 76]. Schulte and coworkers reported that RaGFP displays pK'=6.9 and R_f =8.8 for λ_{x1}= 415 nm, λ_{x2}= 475 nm, and λ_e= 508 nm [78]. In the same work the ratiometric characteristics by emission of EcGFP were also highlighted. Upon excitation at 400 nm,

EcGFP emits at 464 and 511 nm at low and high pH, respectively. Adopting the ratiometric sets (400 nm, 511 nm) and (400, 464), it was found R_f =28 and pK'=7.6 [78].

In 2002, James Remington and its group introduced four new ratiometric pH indicators, named deGFPs, characterized by the S65T and H148C(G) and/or T203C substitutions [55]. The thorough photophysical characterization of deGFPs [55] showed that they retain significant absorption of the neutral state at high pH, suggesting the coupling between residue E222 and the chromophore [43]. pK values were found to range from 6.8 to 8.0 [55]. Remarkably, at low pH, excitation of deGFPs at 400 nm resulted in a broad blue fluorescence centered at 460 nm (Φ=0.05-0.1); conversely, at high pH, the 400 nm-excitation led to green fluorescence (λ_e=516-518 nm, Φ=0.15-0.35). From ultrafast fluorescence upconversion spectroscopy studies, the blue fluorescence was attributed to the direct emission of the excited neutral chromophore, whereas the green fluorescence resulted from an efficient ESPT process [47]. Crystal structure analysis helped to elucidate the basis of the dual emission characteristics through the identification of a pH-induced structural rearrangement in the chromophore pocket [55]. In more detail, at low pH the neutral chromophore did not show ESPT-mediated emission, on account of the interruption of the proton relay towards Glu^{222} typical of wtGFP. Conversely, a raise in pH triggered a backbone motion placing Tyr^{145} and Ser^{147} in a favorable position to form hydrogen bonds with the chromophore hydroxyl; this configuration established a novel proton relay involving Ser^{147} and two water molecules and allowed ESPT towards the bulk solvent. This result is relevant not only for the understanding of deGFPs emission properties, but also because it offers a guiding principle for the engineering of GFP-based ratiometric pH indicators. Indeed, the fine modulation of ESPT rate by rationale modification of the primary sequence appears a very effective method to change the emission properties of GFP mutants [47, 79, 80].

The deGFP4 variant was evaluated as intracellular ratiometric pH indicator by emission (λ_x=

365 nm, λ_{e1}= 475-525 nm, λ_{e2}= 385-470 nm) in the course of the same study. Although no ratiometric parameters were reported, deGFP4 was shown to possess a much greater dynamic range than the popular SNARF-1 dye [81, 82]. The ratio from deGFP4, however, is rather noisy because of the weak fluorescence signal in the blue wavelength range [55]. deGFP4 was also tested as ratiometric indicator by emission under two-photon excitation, a topic that will be discussed in § 7.

In 2006 our group introduced the F64L/S65T/T203Y mutant, named E^2GFP, as a very effective and versatile ratiometric pH indicator for intracellular study.[83] Analogously to deGFPs, E^2GFP displayed a proton-dependent photophysical pattern strongly affected by coupling between the chromophore and Glu^{222} ionization.[43] Differently from deGFPs, however, the neutral chromophore at low pH was found to undergo efficient ESPT upon excitation (λ_e=510 nm, Φ=0.22), although the emission maximum was still significantly blue-shifted compared to the emission generated at higher pH (λ_e=523 nm, Φ=0.91, Fig. 4a). These data should suggest an ESPT mechanism involving changes in the polarity/electronic distribution of the chromophore cavity upon A* deprotonation, because the crystallographic analysis of the ground-state forms and kinetic pH-jump measurements did not highlight any major structural rearrangement upon chromophore ionization [43]. Preliminary theoretical calculations showed that the emission blue-shift may imply the establishment of a H-bonding interaction between the anionic phenol group in the excited state and a residue nearby, possibly His^{148}. Further studies are under way to clarify this relevant point.

In keeping with its spectroscopical properties, E^2GFP was demonstrated to report on intracellular pH ratiometrically by emission with high dynamic range (R_f =5.4 and pK'=7.5 *in vivo* for λ_x= 458 nm, λ_{e1}= 515-600 nm, λ_{e2}= 475-525 nm). Also, E^2GFP was shown to be an excellent ratiometric pH indicator by excitation tailored to imaging setups equipped with widespread Ar-laser excitation sources. The presence of an isosbestic point at 460 nm in the

pH-plot of excitation spectra (Fig. 4b) made us select the 458 nm Ar-line as λ_{x2}, because at this wavelength $F_\infty \approx F_0$ and Eq. 9 predicts a minimal deviation of pK' from pK (6.9 for E^2GFP). Adopting λ_{x1}= 488 nm and λ_e = 500-600 nm we obtained a large dynamic range of measurement *in vivo* (R_f = 10-12) and we were able to observe the cellular alkalinization upon mitosis and the subsequent acidification upon entry in the G1 phase (Fig. 5) [83]. E^2GFP linked to the transactivator protein of HIV-1, Tat, allowed us to determine the pH in nucleolar and promyelocytic leukemia protein (PML) bodies with high spatial resolution [83]. We also observed a significant pH change upon Tat relocation that might be biologically related to the control of HIV-1 transcription [84]. It is worth noting that we found the chloride (and other halides) ion to be a static quencher of E^2GFP fluorescence [85]. As expected by the peculiar dependence of quenching by chloride concentration, however, the ratiometric measurements were not affected at all (Fig. 3) [83].

Recently, our group developed a new ratiometric pH indicator by emission, named E^1GFP, which is spectroscopically similar to E^2GFP but more tailored to mildly acidic intracellular compartments (pK'=6.4-6.6). Also, E^1GFP fluorescence was found to be rather unaffected by chloride ions [85]. Remarkably, we demonstrated that E^1GFP is capable to monitor the vesicle pH in real-time during the multi-step endocytosis through to the intracellular endocytic network [86]. Thus, E^1GFP seems particularly tailored to the detection of *in situ* pH changes involved in dynamic biological phenomena.

So far we discussed only ratiometric indicators constituted by a single-GFP. In 2001 Takeo Awaij and coworkers developed two ratiometric pH sensors (GFpH and YFpH) by fusing in tandem two GFP variants having different pH sensitivities [87]. GFpH was constituted by GFPuv, a mutant that displays a low pH-sensitivity and is excitable at 380 nm, and EGFP. The fluorescence of GFpH at 380 and 480 nm excitation was attributed to GFPuv and EGFP, respectively, and in both cases emission at 510 nm is obtained. GFpH displayed pK'=6.2 and $R_f \approx 5$, suggesting its use as ratiometric pH indicator by excitation for mildly acidic

subcellular components [87]. YFpH was constituted by GFPuv and EYFP. Upon 380 nm excitation, the emission of YFpH was shifted from 509 nm to 527 nm as the pH was raised. This effect was interpreted as FRET between GFPuv and EYFP, as EYFP is not fluorescent when excited at 380 nm. Conversely, upon 480 nm excitation the emission of YFpH was nearly unchanged, as it derived mostly from EYFP. On account of this behavior, YFpH was proposed as a ratiometric pH indicator by excitation and by emission. The pK' was shown to be around 6.5-6.8 in both cases [87]. Both GFpH and YFpH were used to visualize pH changes in the cytosol/nucleus of living cells and during internalization caused by endocytosis upon agonist stimulation [87].

Cyan Fluorescent Protein and EYFP are two variants widely used for *in vivo* FRET experiments, owing to their large optical complementarity [88, 89]. Differently to EYFP, CFP is not very sensitive to pH [44], and therefore the CFP-EYFP (or EYFP variants) couple has been proposed as ratiometric pH indicator by excitation and/or emission, likewise the YFpH construct. CFP-EYFP has been shown to possess pK=6.5 and has been used to detect changes in pH secondary to H^+ efflux into the basolateral space of MDCK cells [90]. Pozzan and coworkers developed an indicator by excitation for the high-pH range (mtAlpHi) by replacing the calmodulin linker of the Ca^{2+}-sensor camgaroo-II [74] with a portion of aequorin. mtAlpHi was targeted to mildly alkaline mithochondria and was used to monitor pH changes occurring in a variety of physiological and non-physiological situations [13]. Notably, mtAlpHi (and its parent construct camgaroo-II) comprises an EYFP variant that is poorly sensitive to the quenching effects of chloride ions [74]. Nonetheless, the EYFP sensitivity to Cl^- was exploited to engineer CFP-EYFP ratiometric indicators of both proton and chloride ions [91].

7. Instrumentation and methods for the pH detection *in vivo*

The detection of pH in cultured cells and living organisms has greatly benefited from the recent developments of highly effective microimaging setups and first of all of the confocal microscope [81, 92, 93]. In a confocal microscope, the fluorescence from out-of-focus optical planes is virtually fully eliminated by the presence of a pinhole in an optically conjugate plane in front of the detector [94]. By means of this configuration, the image quality and the axial resolution are greatly improved compared to conventional (e.g. wide-field) epifluorescence microscopes. For high numerical-aperture objectives, the axial resolution (z-axis) can be as low as 0.6-1.5 μm (the xy resolution is usually around 0.2-0.5 μm). Thus, confocal microscopy allows for pH detection in focal volumes of less than 1 fl and provides a very effective way to obtain high-resolution pH maps in living organisms such as cultured cells. Nonetheless, the pH determination is always based on the high-sensitivity detection of fluorescence, a common issue for any microimaging setup. Different aspects are to be discussed according to the properties of the fluorescent probes, in particular ifit is ratiometric or not.

As described in the text, non-ratiometric pH indicators are employed normally to monitor pH variations *in vivo* following some external stimuli. Measurements of this kind require a stable source of excitation and the capability to reveal fluorescence-emission changes in the presence of a background noise and/or autofluorescence. Hence, any means aimed at maximizing the signal-to-noise ratio (SNR) must be pursued; examples are highly-selective excitation/dichroic/emission filters, high photon fluxes of excitation (compatible with the bleaching properties of the indicator), and sensitive detectors to reveal weak signals.

The measurements by ratiometric indicators need additional considerations. First of all, the microimaging system must be flexible in selecting, and fast in switching, the excitation sources and/or the collection intervals, in dependence of the ratiometric nature of the probe. It

is worth saying that even standard confocal microscopes are usually supplied with multiple excitation laser sources that can be activated sequentially in less than 100 ms, and are therefore well-suited for the excitation ratiometry experiment. Note, however, that the typical laser source for GFP excitation, the Ar ion laser, provides only few excitation wavelengths. In this regard, E^2GFP is an optimized indicator for confocal imaging, as it works at its best when excited at 458 and 488 nm, two strong lines of Ar laser (§ 5 [83]). Some wide-field microscopes can be interfaced with motorized filter wheels that allow the fast switching of excitation wavelengths from a lamp source. In this case, the excitation interval is tunable, although the high resolution of confocal setups is lost (and can be recovered only by post-processing deconvolution).

Confocal microscopes are typically supplied with multiple photomultiplier detectors. This allows the concomitant collection of fluorescence in at least two wavelength intervals, which is the basic requirement of ratiometry by emission. In the most advanced setups the fluorescence collection of each detector can be tuned to a desired wavelength interval directly from the software, which controls a complex system of gratings and slits within the microscope (bandwidths can be as low as 5 nm). This instrumental feature is particularly interesting in view of modulating both the dynamic range and the apparent pK' of ratiometric response (§ 4, eq. 5-9).

Minimization of the detector noise (image background) is of utmost relevance for ratiometric measurements. Indeed, the ratio between fluorescence values amplifies the electronic error present in each image. The non-linear (sigmoidal) shape of the calibration curve further amplifies this error when the ratio is converted to pH. Some detectors have an intrinsically-high noise level (e.g.: SPAD), but also conventional PMTs may display strong image backgrounds when the fluorescence signal is low and the detector gain is high. Thus, the maximum excitation intensity compatible with minimal probe photobleaching should always be adopted during measurements. After collection, adequate thresholding of images (by

means of some reproducible criteria, e.g. the subtraction of background plus a fixed multiple of its standard deviation) is vital to obtain a meaningful pH map.

Finally, it is worth noting that the use of photon-counting detectors represents an interesting option to carry out ratiometric measurements, as they are characterized by predictable and low-level Poissonian noise [95]. These detectors, however, are usually part of complex setups devoted to high-sensitivity biophysical measurements and are not components of standard instruments. Nonetheless, we are currently trying to implement this technique for ratiometric measurements by emission with our new pH indicator E^{1}GFP (§ 6).

8. Future developments: multiphoton-excitable pH indicators based on GFPs

Multiphoton microscopy has found a wide use in the world of biological imaging as the best noninvasive means of fluorescence microscopy in tissue explants and living animals [96, 97]. This is a laser scanning technique that exploits the supralinear power-intensity dependence of the excitation in order to excite fluorescence only within the focal region of the excitation beam. For this reason, phototoxicity and photobleaching are reduced with respect to single-photon excitation confocal microscopy. Furthermore, nonlinear optical microscopy allows large depth penetration in biological tissues, as scattered signal photons can be assigned to their origin as the result of localized nonlinear signal generation and there is a window of minimum “linear” absorption by water and biomolecules in the near infrared. Therefore, fluorescent indicators that respond to non-linear excitation are very desirable, in order to gain high spatial penetration depths in turbid and highly scattering biological specimens and pH indicators make no exceptions. It is worth noting that many commercially available confocal setups can be easily upgraded to multiphoton imaging by interfacing a femto- or pico-second mode-locked infrared laser source [96]. Some of these sources, though more expensive, are

totally controlled by software and do not require time-consuming manual tuning/mode-locking of the excitation wavelength.

As anticipated in § 6, Remington and coworkers established the good performance of deGFPs, in particular of deGFP4, as two-photon (2P) ratiometric pH indicator by emission [55]. Significantly, 2P excitation microscopy provided a superior signal-over-background level compared with one-photon excitation at 364 nm, in particular for the blue emission. They attributed the improved signal over background to decreased cellular autofluorescence and/or more efficient excitation of the protonated deGFP4 in response to 810 nm excitation.

We found that also E^2GFP has the potential to be a 2P ratiometric pH indicator, by both excitation and emission. Preliminary 2P experiments on this protein were carried out by Chirico and coworkers [98, 99]. In their work they studied the fluorescence and the photoconversion of the protein at single molecule level, by trapping it inside silica gels with pores of dimensions of the order of the proteins. Interestingly, they reported the number of detected proteins whose emission derived from the neutral and anionic chromophore as a function of pH, obtaining pK≈6.5 for chromophore protonation. In view of assessing the pH dependence also in bulk, we carried out two-photon measurements of E^2GFP in solution using a tunable IR laser coupled to a confocal microscope. Preliminary unpublished excitation (i.e. cross section σ_{TPE} *vs* wavelength plots) and emission spectra are reported in Fig. 6 for the pH 4.9, 7 and 9.5. Both spectra were normalized by using fluorescein at pH~12 as standard. σ_{TPE} has been obtained as:

$$\sigma_{TPE} = \frac{C_{cal}(F - F_{back})}{C_p(F_{cal} - F_{back})} \sigma_{TPE}^{cal} \quad [13]$$

where F and F_{cal} are the detected fluorescence intensities of the sample and of the fluorescein, F_{back} is the background signal, C_p and C_{cal} are the protein and fluorescein concentrations and $\sigma_{\mathrm{TPE}}^{cal} = 0.9\sigma_{\mathrm{TPA}}^{cal}$ where $\sigma_{\mathrm{TPA}}^{cal}$ is the fluorescein two-photon absorption cross section and 0.9 is its quantum yield [100]. This calibration method does not require the knowledge of the second-order temporal coherence of the beam, which depends on the spatial and temporal intensity profile of the excitation pulses [100, 101].

The 2P-excitation spectra displayed in Figure 6a are similar to the excitation spectra obtained by one-photon excitation at half wavelength (Fig. 4b). Remarkably, σ_{TPE} below 880nm was found to decrease as pH was raised, while σ_{TPE} above 930 nm showed the opposite trend. Thus, E^2GFP appears suitable as 2P pH indicator ratiometric by excitation. Furthermore, excitation at 780 nm led to the red-shift of the emission band upon pH rise. The ratio of the energy emitted in the wavelength ranges indicated in Fig. 6b as shaded areas (520-550 nm and 475-505 nm) was found to increase by a factor of 3 when pH was shifted from 4.9 up to 9.5. On account of these data, E^2GFP seems suitable also as 2P pH indicator ratiometric by emission. Nonetheless, more analysis is needed in order to find the optimum excitation wavelength and emission ranges, and to explain the details of the small differences between the photophysics of "linearly" and "non-linearly" excited E^2GFP.

Conclusions

Fluorescent proteins, and particularly the members of the *Aequorea Victoria* family (GFPs), have become the most important fluorescent probes to monitor biochemical processes *in vivo*. The fluorescence of GFPs is genetically encoded in the protein's primary sequence and can be monitored in living specimens by fluorescence microscopy. Fusion constructs of GFPs and target proteins are easily engineered by standard methods of molecular biology. Thus, GFPs

represent an excellent way to look at the intracellular fate of target protein biomolecules in real time.

Remarkably, the presence of a phenol ionizable group on the GFP chromophore leads to two protonation ground states (neutral and anionic) that display considerably different absorption and fluorescence excitation (and sometime, emission) characteristics. This peculiar spectroscopic feature prompted the use of several GFPs as fluorescent indicators of intracellular pH. In few cases the photophysics of the GFP mutants allowed the engineering of ratiometric pH indicators, either by excitation or by emission. Ratiometric indicators represent the most useful class of fluorescent sensors, as they do not require each time an independent determination of their concentration , allowing therefore a universal calibration within a series of experiments. In this review, we examined the main GFP-based indicators developed so far, discussing their properties and their reported applications. Yet, no indicator reported so far is satisfactory for all *in vivo* uses, and any selection requires the knowledge of the photophysical features of the probe and their compatibility with the envisaged application and imaging setup.

The engineering of new optimized pH indicators is a stimulating task from a biophysical perspective, and requires a thorough knowledge of the protonation reactions of the chromophore and nearby residues in the protein structure. Here, two aspects are to be considered: the thermodynamic tendency of the chromophore to ionization (i.e., the pK) and the spectroscopic properties of the neutral and anionic chromophore forms. Concerning the pK, we showed that it is often the result of a thermodynamic balance between the deprotonation reaction of the chromophore and a nearby residue(s). For both moieties, the introduction/removal of aminoacids capable to stabilize the neutral/anionic forms via H-bonding (e.g.: Thr^{203} to stabilize the anionic chromophore) is an efficient way to tune finely the pK of the optical response.

Tailoring of the spectral characteristics of the neutral and anionic chromophore forms is less prone to a general approach. The anionic state is usually very bright, and its excitation/emission is somewhat susceptible to changes in polarity/electronic density of the chromophore cavity (e.g: the yellow emission of Y203 mutants [71]). The neutral chromophore may undergo two emission pathways: direct emission from its excited state ($\lambda_{em} \approx 460$ nm, [48]), or ESPT to yield an excited state more similar to that of the anionic chromophore ($\lambda_{em} > 500$ nm). The ESPT mechanism requires an efficient proton relay towards a final acceptor, and its rate can be tuned by modifying the aminoacids that take part in this proton relay [102]. Note that changes in ESPT rate can affect both the wavelength and the yield of emission.

Finally, GFP mutants that display pH-dependent large shifts in emissions are ideally suited to act as multiphoton pH-indicators. Owing to the increasing relevance that multiphoton imaging has in the biological field, we described in the final chapter the GFP variants that were reported as efficient two-photon pH indicators, presenting also some preliminary, unpublished, results of ours.

ACKNOWLEDGMENTS

We thank Dr. Riccardo Nifosì (Scuola Normale Superiore) for stimulating discussions.

Authors also gratefully acknowledge the partial financial support of the Italian Ministry for University and Research (FIRB No. RBLA03ER38).

REFERENCES

1. Srivastava, J, Barber, DL, Jacobson, MP (2007) Physiology (Bethesda, Md 22:30-39.

2. Wang, H, Singh, D, Fliegel, L (1997) J Biol Chem 272:26545-26549.

3. Putney, LK, Barber, DL (2003) J Biol Chem 278:44645-44649.

4. Fliegel, L (2005) Int J Biochem Cell Biol 37:33-37.

5. Hunte, C, Screpanti, E, Venturi, M, Rimon, A, Padan, E, Michel, H (2005) Nature 435:1197-1202.

6. Wakabayashi, I, Poteser, M, Groschner, K (2006) Journal of vascular research 43:238-250.

7. Sun, HY, Wang, NP, Halkos, ME, Kerendi, F, Kin, H, Wang, RX, Guyton, RA, Zhao, ZQ (2004) Eur. J. Pharmacol. 486:121-131.

8. Denker, SP, Barber, DL (2002) J Cell Biol 159:1087-1096.

9. Kapus, A, Szaszi, K, Sun, J, Rizoli, S, Rotstein, OD (1999) J Biol Chem 274:8093-8102.

10. Mellman, I, Warren, G (2000) Cell 100:99-112.

11. Rybak, SL, Lanni, F, Murphy, RF (1997) Biophys J 73:674-687.

12. Jahn, R, Lang, T, Sudhof, TC (2003) Cell 112:519-533.

13. Abad, MFC, Di Benedetto, G, Magalhaes, PJ, Filippin, L, Pozzan, T (2004) J. Biol. Chem. 279:11521-11529.

14. Carnell, L, Moore, HP (1994) J Cell Biol 127:693-705.

15. Chanat, E, Huttner, WB (1991) J Cell Biol 115:1505-1519.

16. Puri, S, Bachert, C, Fimmel, CJ, Linstedt, AD (2002) Traffic 3:641-653.

17. Kellokumpu, S, Sormunen, R, Kellokumpu, I (2002) FEBS Lett 516:217-224.

18. Lakowicz, JR (1999) Principles of Fluorescence Spectroscopy. Plenum US, Oakland.

19. Rink, TJ, Tsien, RY, Pozzan, T (1982) J Cell Biol 95:189-196.

20. Tsien, RY (1989) Methods in cell biology 30:127-156.

21. Lin, HJ, Herman, P, Lakowicz, JR (2003) Cytom. Part A 52A:77-89.

22. Shimomura, O, Johnson, FH, Saiga, Y (1962) J Cell Comp Physiol 59:223-239.

23. Tsien, RY (1998) Annu. Rev. Biochem. 67:509-544.

24. Prasher, DC, Eckenrode, VK, Ward, WW, Prendergast, FG, Cormier, MJ (1992) Gene 111:229-233.

25. Chalfie, M, Tu, Y, Euskirchen, G, Ward, WW, Prasher, DC (1994) Science 263:802-805.

26. Chudakov, DM, Lukyanov, S, Lukyanov, KA (2005) Trends Biotechnol 23:605-613.

27. Miyawaki, A (2005) Neuron 48:189-199.

28. Shaner, NC, Steinbach, PA, Tsien, RY (2005) Nat. Methods 2:905-909.

29. Zhang, J, Campbell, RE, Ting, AY, Tsien, RY (2002) Nat. Rev. Mol. Cell. Biol. 3:906-918.

30. Ormo, M, Cubitt, AB, Kallio, K, Gross, LA, Tsien, RY, Remington, SJ (1996) Science 273:1392-1395.

31. Wachter, RM (2007) Acc Chem Res 40:120-127.

32. Niwa, H, Inouye, S, Hirano, T, Matsuno, T, Kojima, S, Kubota, M, Ohashi, M, Tsuji, FI (1996) Proc. Natl. Acad. Sci. 93:13617-13622.

33. Webber, NM, Litvinenko, KL, Meech, SR (2001) J. Phys. Chem. B 105:8036-8039.

34. Ward, WW, Bokman, SH (1982) Biochemistry 21:4535-4540.

35. Brejc, K, Sixma, TK, Kitts, PA, Kain, SR, Tsien, RY, Ormo, M, Remington, SJ (1997) Proc. Natl. Acad. Sci. 94:2306-2311.

36. Kummer, AD, Wiehler, J, Rehaber, H, Kompa, C, Steipe, B, Michel-Beyerle, ME (2000) J. Phys. Chem. B 104:4791-4798.

37. Wachter, RM, Yarbrough, D, Kallio, K, Remington, SJ (2000) J. Mol. Biol. 301:157-171.

38. Sniegowski, JA, Lappe, JW, Patel, HN, Huffman, HA, Wachter, RM (2005) J. Biol. Chem. 280:26248-26255.

39. Zhang, L, Patel, HN, Lappe, JW, Wachter, RM (2006) J Am Chem Soc 128:4766-4772.

40. Bell, AF, He, X, Wachter, RM, Tonge, PJ (2000) Biochemistry 39:4423-4431.

41. Dong, J, Solntsev, KM, Tolbert, LM (2006) J Am Chem Soc 128:12038-12039.

42. Elsliger, MA, Wachter, RM, Hanson, GT, Kallio, K, Remington, SJ (1999) Biochemistry 38:5296-5301.

43. Bizzarri, R, Nifosi, R, Abbruzzetti, S, Rocchia, W, Guidi, S, Arosio, D, Garau, G, Campanini, B, Grandi, E, Ricci, F, Viappiani, C, Beltram, F (2007) Biochemistry 46:5494-5504.

44. Llopis, J, McCaffery, JM, Miyawaki, A, Farquhar, MG, Tsien, RY (1998) Proc. Natl. Acad. Sci. 95:6803-6808.

45. Voityuk, AA, Michel-Beyerle, ME, Rosch, N (1998) Chem. Phys. 231:13-25.

46. Chattoraj, M, King, BA, Bublitz, GU, Boxer, SG (1996) Proc. Natl. Acad. Sci. 93:8362-8367.

47. McAnaney, TB, Park, ES, Hanson, GT, Remington, SJ, Boxer, SG (2002) Biochemistry 41:15489-15494.

48. Bonsma, S, Purchase, R, Jezowski, S, Gallus, J, Konz, F, Volker, S (2005) ChemPhysChem 6:838-849.

49. Creemers, TM, Lock, AJ, Subramaniam, V, Jovin, TM, Volker, S (1999) Nat Struct Biol 6:557-560.

50. Wiehler, J, Jung, G, Seebacher, C, Zumbusch, A, Steipe, B (2003) ChemBioChem 4:1164-1171.

51. Kennis, JT, Larsen, DS, van Stokkum, IH, Vengris, M, van Thor, JJ, van Grondelle, R (2004) Proc. Natl. Acad. Sci. 101:17988-17993.

52. Lukyanov, KA, Chudakov, DM, Fradkov, AF, Labas, YA, Matz, MV, Lukyanov, S (2006) Methods Biochem Anal 47:121-138.

53. Kneen, M, Farinas, J, Li, Y, Verkman, AS (1998) Biophys. J. 74:1591-1599.

54. Abbruzzetti, S, Grandi, E, Viappiani, C, Bologna, S, Campanini, B, Raboni, S, Bettati, S, Mozzarelli, A (2005) J. Am. Chem. Soc. 127:626-635.

55. Hanson, GT, McAnaney, TB, Park, ES, Rendell, ME, Yarbrough, DK, Chu, S, Xi, L, Boxer, SG, Montrose, MH, Remington, SJ (2002) Biochemistry 41:15477-15488.

56. Ullmann, GM (2003) J. Phys. Chem. B 107:1263-1271.

57. Grynkiewicz, G, Poenie, M, Tsien, RY (1985) J Biol Chem 260:3440-3450.

58. Sonnleitner, A, Schutz, GJ, Schmidt, T (1999) Biophys J 77:2638-2642.

59. Digman, MA, Brown, CM, Sengupta, P, Wiseman, PW, Horwitz, AR, Gratton, E (2005b) Biophys J 89:1317-1327.

60. Cardarelli, F, Serresi, M, Bizzarri, R, Beltram, F (2008) Traffic 9:528-539.

61. Cardarelli, F, Serresi, M, Bizzarri, R, Giacca, M, Beltram, F (2007) Mol Ther 15:1313-1322.

62. Hell, SW (2003) Nat Biotechnol 21:1347-1355.

63. Haupts, U, Maiti, S, Schwille, P, Webb, WW (1998) Proc. Natl. Acad. Sci. 95:13573-13578.

64. Bosisio, C, Quercioli, V, Collini, M, D'Alfonso, L, Baldini, G, Bettati, S, Campanini, B, Raboni, S, Chirico, G (2008) J Phys Chem B 112:8806-8814.

65. Widengren, J, Terry, B, Rigler, R (1999) Chem. Phys. 249:259-271.

66. Charier, S, Meglio, A, Alcor, D, Cogne-Laage, E, Allemand, JF, Jullien, L, Lemarchand, A (2005) J Am Chem Soc 127:15491-15505.

67. Sankaranarayanan, S, De Angelis, D, Rothman, JE, Ryan, TA (2000) Biophys. J. 79:2199-2208.

68. Nakabayashi, T, Wang, HP, Kinjo, M, Ohta, N (2008) Photochem Photobiol Sci 7:668-670.

69. Miesenbock, G, De Angelis, DA, Rothman, JE (1998) Nature 394:192-195.

70. Hess, ST, Heikal, AA, Webb, WW (2004) J. Phys. Chem. B 108:10138-10148.

71. Wachter, RM, Elsliger, MA, Kallio, K, Hanson, GT, Remington, SJ (1998) Structure 6:1267-1277.

72. Patterson, G, Day, RN, Piston, D (2001) J Cell Sci 114:837-838.

73. Jayaraman, S, Haggie, P, Wachter, RM, Remington, SJ, Verkman, AS (2000) J. Biol. Chem. 275:6047-6050.

74. Griesbeck, O, Baird, GS, Campbell, RE, Zacharias, DA, Tsien, RY (2001) J Biol Chem 276:29188-29194.

75. Karagiannis, J, Young, PG (2001) J Cell Sci 114:2929-2941.

76. Jankowski, A, Kim, JH, Collins, RF, Daneman, R, Walton, P, Grinstein, S (2001) J Biol Chem 276:48748-48753.

77. Machen, TE, Leigh, MJ, Taylor, C, Kimura, T, Asano, S, Moore, HP (2003) American journal of physiology 285:C205-214.

78. Schulte, A, Lorenzen, I, Bottcher, M, Plieth, C (2006) Plant methods 2:7.

79. Shu, X, Leiderman, P, Gepshtein, R, Smith, NR, Kallio, K, Huppert, D, Remington, SJ (2007) Protein Sci 16:2703-2710.

80. Shu, X, Kallio, K, Shi, X, Abbyad, P, Kanchanawong, P, Childs, W, Boxer, SG, Remington, SJ (2007) Biochemistry 46:12005-12013.

81. Cody, SH, Dubbin, PN, Beischer, AD, Duncan, ND, Hill, JS, Kaye, AH, Williams, DA (1993) Micron 24:573-580.

82. Dubbin, PN, Cody, SH, Williams, DA (1993) Micron 24:581-586.

83. Bizzarri, R, Arcangeli, C, Arosio, D, Ricci, F, Faraci, P, Cardarelli, F, Beltram, F (2006) Biophys. J. 90:3300-3314.

84. Marcello, A, Lusic, M, Pegoraro, G, Pellegrini, V, Beltram, F, Giacca, M (2004) Gene 326:1-11.

85. Arosio, D, Garau, G, Ricci, F, Marchetti, L, Bizzarri, R, Nifosi, R, Beltram, F (2007) Biophys J 93:232-244.

86. Serresi, M, Bizzarri, R, Cardarelli, F, Beltram, F (2009) Anal Bioanal Chem, *accepted* (DOI: 10.1007/s00216-008-2489-7)

87. Awaji, T, Hirasawa, A, Shirakawa, H, Tsujimoto, G, Miyazaki, S (2001) Biochem. Biophys. Res. Commun. 289:457-462.

88. Chan, FK, Siegel, RM, Zacharias, D, Swofford, R, Holmes, KL, Tsien, RY, Lenardo, MJ (2001) Cytometry 44:361-368.

89. Wlodarczyk, J, Woehler, A, Kobe, F, Ponimaskin, E, Zeug, A, Neher, E (2008) Biophys J 94:986-1000.

90. Urra, J, Sandoval, M, Cornejo, I, Barros, LF, Sepulveda, FV, Cid, LP (2008) Pflugers Arch.

91. Markova, O, Mukhtarov, M, Real, E, Jacob, Y, Bregestovski, P (2008) Journal of neuroscience methods 170:67-76.

92. Tsien, RY (2003) Nat Rev Mol Cell Biol Suppl:SS16-21.

93. Paddock, S (2008) BioTechniques 44:643-644, 646, 648.

94. Diaspro, A, Bianchini, P, Vicidomini, G, Faretta, M, Ramoino, P, Usai, C (2006) Biomedical engineering online 5:36.

95. Digman, MA, Dalal, R, Horwitz, AF, Gratton, E (2008) Biophys J 94:2320-2332.

96. Zipfel, WR, Williams, RM, Webb, WW (2003) Nat Biotechnol 21:1369-1377.

97. Svoboda, K, Yasuda, R (2006) Neuron 50:823-839.

98. Chirico, G, Diaspro, A, Cannone, F, Collini, M, Bologna, S, Pellegrini, V, Beltram, F (2005) ChemPhysChem 6:328-335.

99. Chirico, G, Cannone, F, Diaspro, A, Bologna, S, Pellegrini, V, Nifosi, R, Beltram, F (2004) Phys. Rev. E 70.

100. Albota, MA, Xu, C, Webb, WW (1998) Appl. Opt. 37:7352-7356.

101. Heikal, A, Hess, S, Webb, WW (2001) Chem. Phys. 274:37-55.

102. Stoner-Ma, D, Jaye, AA, Ronayne, KL, Nappa, J, Meech, SR, Tonge, PJ (2008) J Am Chem Soc 130:1227-1235.

CAPTIONS TO FIGURES AND SCHEMES

Fig. 1 3D structure (β-can) of wt-GFP from X-ray analysis [30]. The chromophore (colored) is buried at center of the β-can structure.

Fig. 2 (a) Absorption spectra of F64L/S65T GFP at different pH values. Note that A state (λ=395 nm) is progressively converted to B state (λ =486 nm) as pH is raised. (b) Sigmoidal trend of fluorescence (λ_x=486 nm, λ_e=509 nm) *vs* pH for F64L/S65T GFP (blue points); the experimental data were fit to Eq. 3 (dashed red line), obtaining pK=5.7.

Fig. 3 Ratiometric plot (general calibration curve) for F64L/S65T/T203Y GFP (E^2GFP). Experimental points (blue) were fitted to Eq. 5 (dashed red curve) and the graphical meanings of the ratiometric parameters are added. The two excitation/collection sets are: (λ_x=488 nm,λ_e=523 nm) and (λ_x=458 nm,λ_e=523 nm). Notably, all measurements were carried out *in vitro* and each point is an average of R[1,2] taken at different chloride concentrations (0-200 mM) to display ratiometric independence from this fluorescence quencher.

Fig. 4 (a) Emission (λ_x=473 nm) and (b) excitation (λ_x =523 nm) spectra of E^2GFP at four different pH values. Note that the isosbestic points in both series that indicate pH-dependent equilibrium between two forms.

Fig. 5 Intracellular pH monitored by E^2GFP during mitosis [83]. Left: fluorescence intensity image (λ_x =488 nm, λ_e =500-600 nm). Right: pH map according to the ratiometric excitation sets (488, 500-600) (458, 500-600). Note the progressive cell alkalinization upon division (Time = 0' to 18') and subsequent acidification upon entry in the G1 phase (Time = 21' to 110').

Fig 6 (a) 2-photon-action cross-sections σ_{TPE} in GM units (1 GM=10^{-50} cm^4 s/photon) of E^2GFP (at pH = 4.9, 7.0 and 9.5) over the 730–960 nm excitation range, with fluorescence emission in the range 450–650 nm. Error bars are estimated as standard deviations of the results of 4 to 10 measurements, often at different excitation intensities. (b) Fluorescence emission spectra of E^2GFP, excited by 2-photon absorption at 780nm, at pH = 4.9, 7.0 and 9.5. The shaded areas highlight two wavelength ranges where emission should be detected in order to use E^2GFP as a 2P ratiometric pH indicator by emission.

Scheme 1 Protonation equilibria accessible to the GFP chromophore. The four possible states are denoted as neutral or A (**I**), anionic or B (**II**), cationic (**III**), and zwitterionic (**IV**)

Scheme 2 Protonation equilibrium at basis of the pH dependence of GFPs' optical response

Scheme 3 The 2S model of pH-dependent ground states in GFPs. X is an ionizable residue locate in close proximity to the chromophore. When X and the chromophore are uncoupled, only equilibrium **A'↔B** is relevant to the optical properties of the protein. When the two sites are coupled, their ionizations inhibit one another (strong anticooperative coupling). In such a case, the **B'** state is populated at pH beyond the stability range of the protein: a pseudo single-site ionization behavior ensues [43].

FIGURE 1

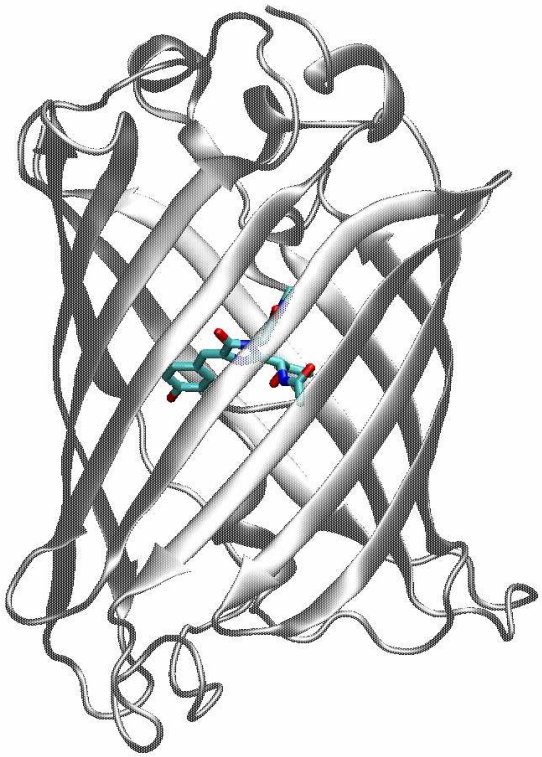

FIGURE 2

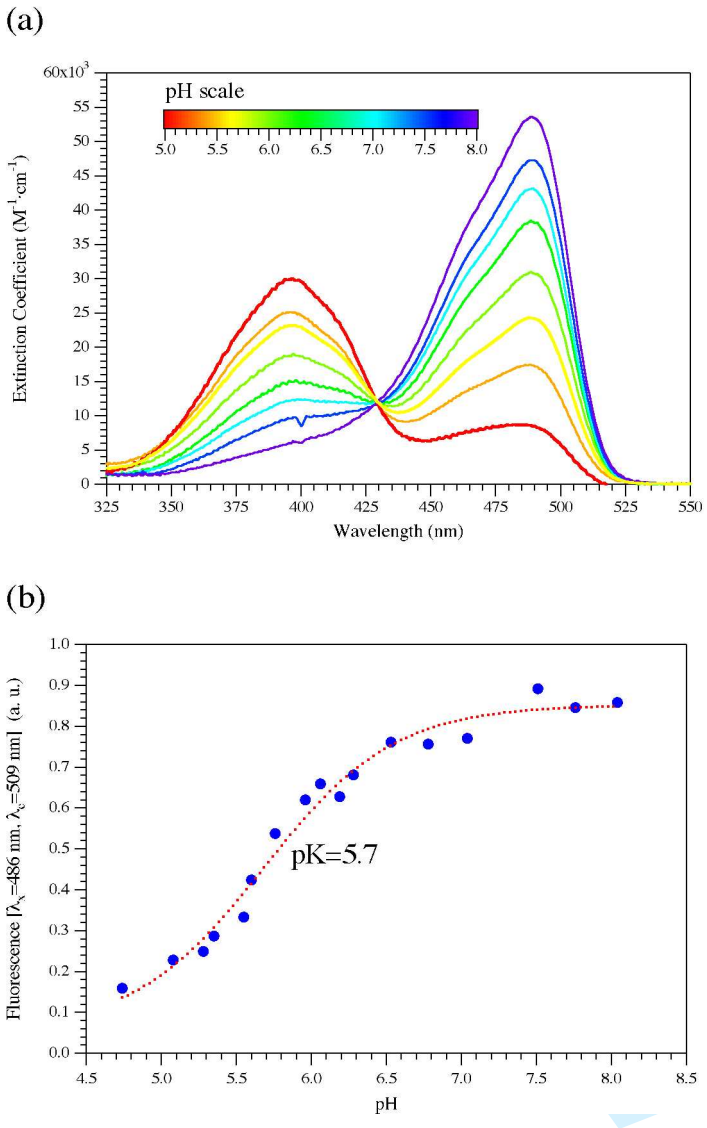
(a)
pH scale
5.0 5.5 6.0 6.5 7.0 7.5 8.0
Extinction Coefficient (M-1·cm-1)
60x10³
55
50
45
40
35
30
25
20
15
10
5
0
325 350 375 400 425 450 475 500 525 550
Wavelength (nm)
(b)
Fluorescence [λx=486 nm, λe=509 nm] (a. u.)
1.0
0.9
0.8
0.7
0.6
0.5
0.4
0.3
0.2
0.1
0.0
pK=5.7
4.5 5.0 5.5 6.0 6.5 7.0 7.5 8.0 8.5
pH

FIGURE 3

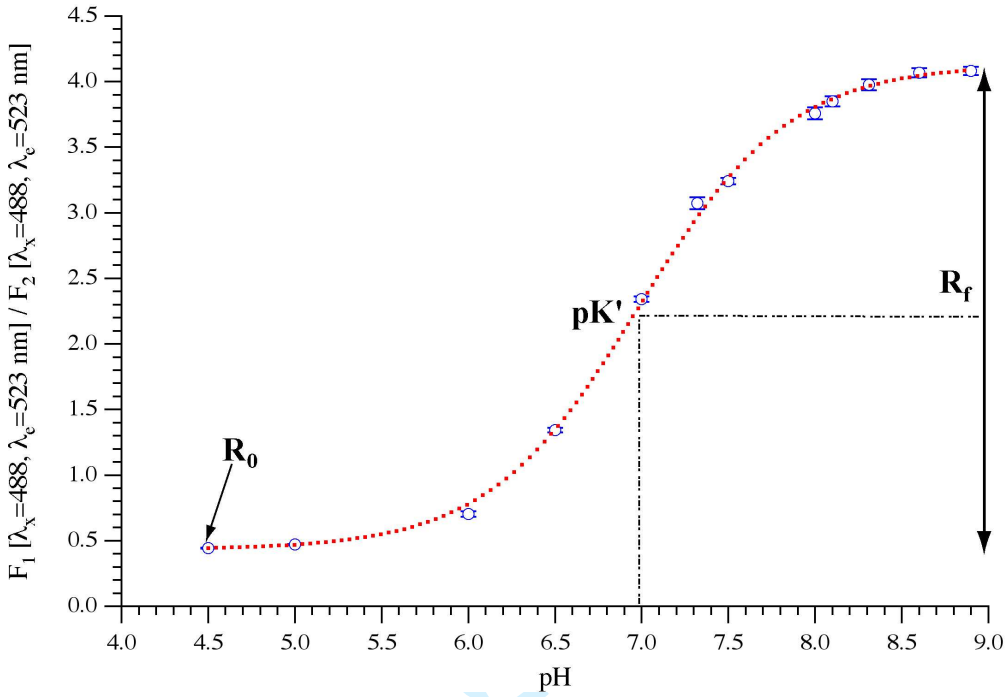

FIGURE 4

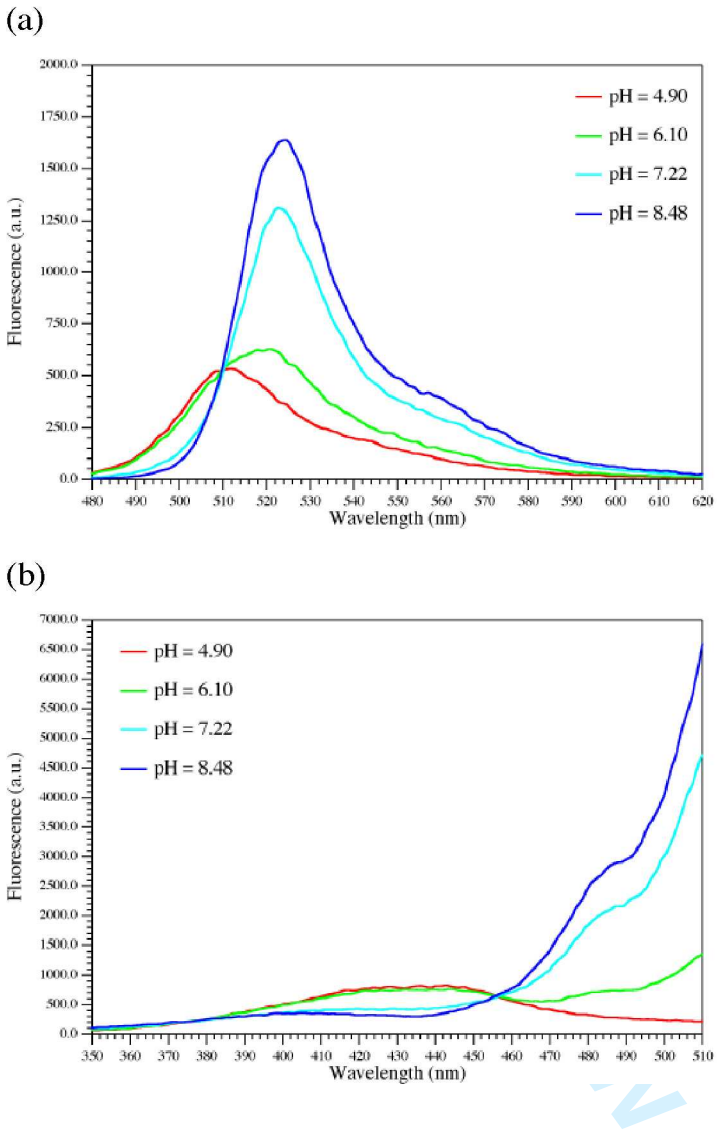
(a)
pH = 4.90
pH = 6.10
pH = 7.22
pH = 8.48
Fluorescence (a.u.)
Wavelength (nm)
(b)
pH = 4.90
pH = 6.10
pH = 7.22
pH = 8.48
Fluorescence (a.u.)
Wavelength (nm)

FIGURE 5

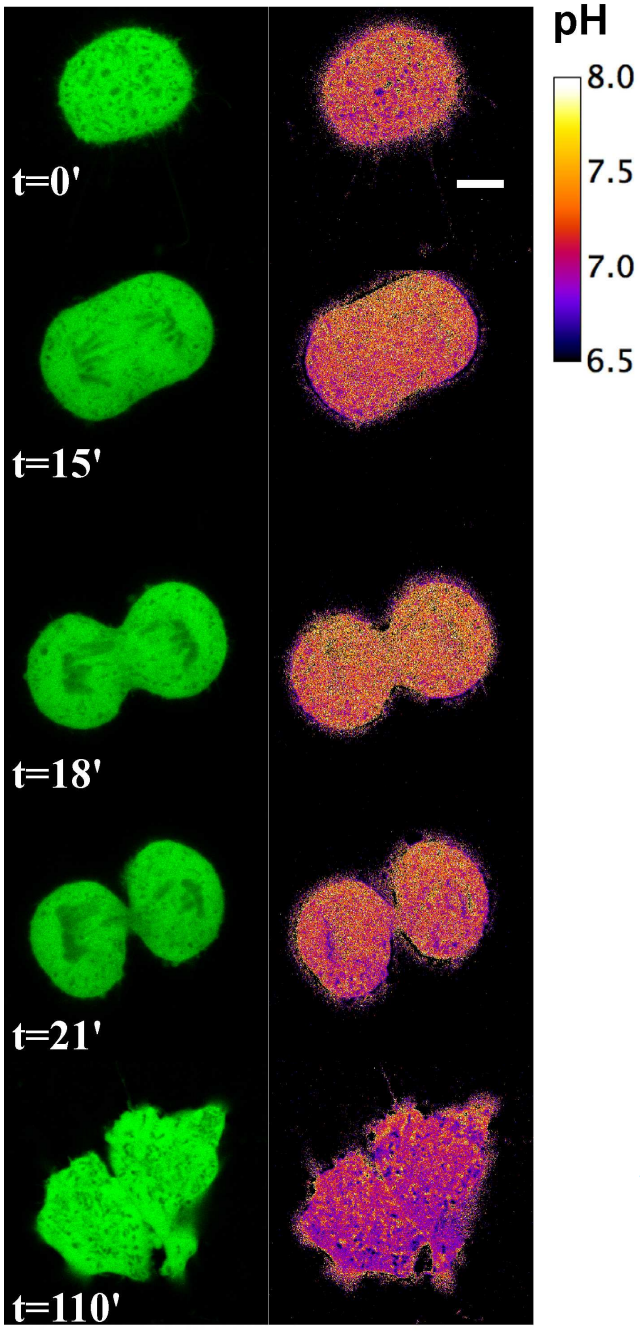

FIGURE 6

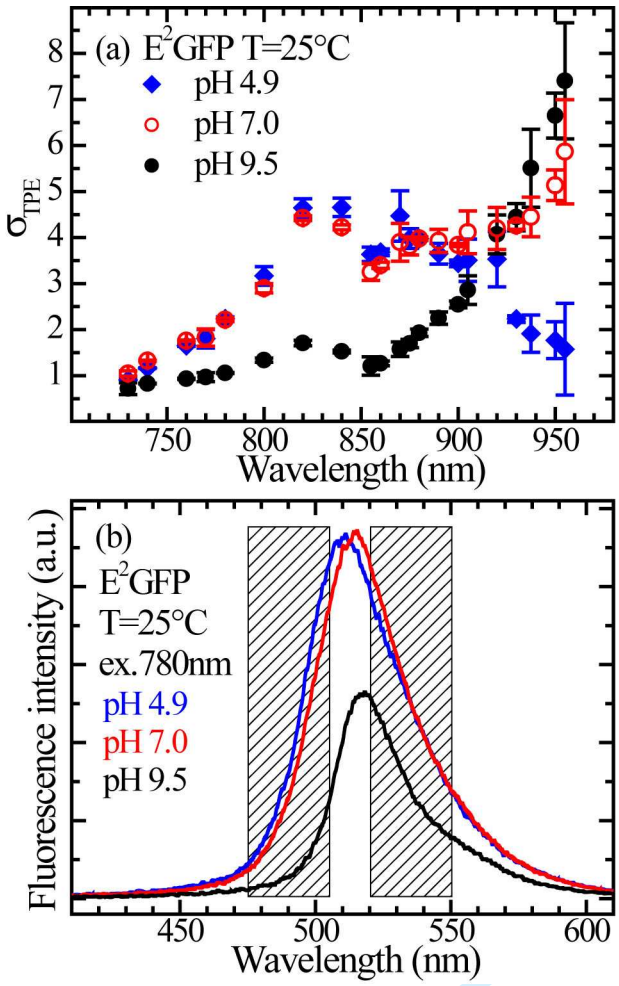
(a) E²GFP T=25°C
pH 4.9
pH 7.0
pH 9.5
σTPE
Wavelength (nm)
(b)
E²GFP
T=25°C
ex.780nm
pH 4.9
pH 7.0
pH 9.5
Fluorescence intensity (a.u.)
Wavelength (nm)

SCHEME 1

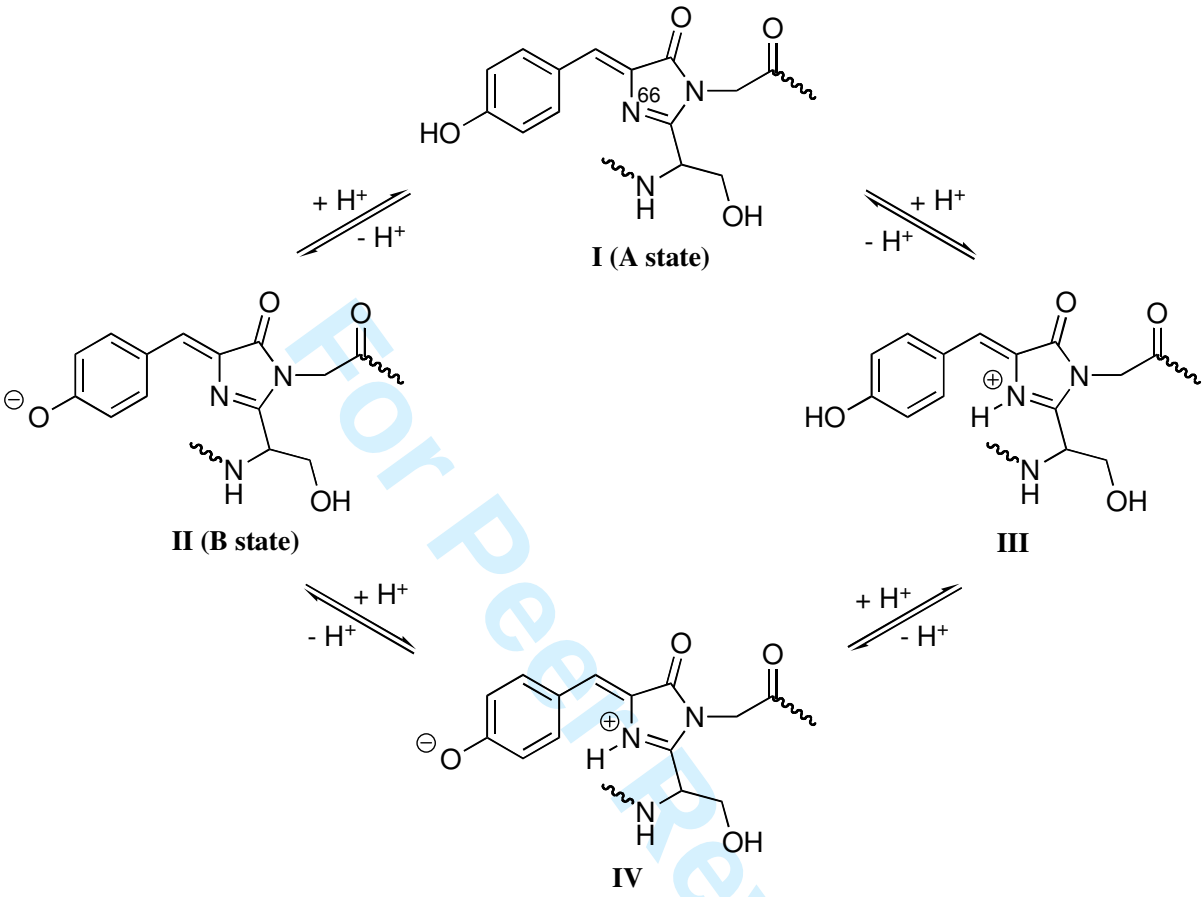

SCHEME 2

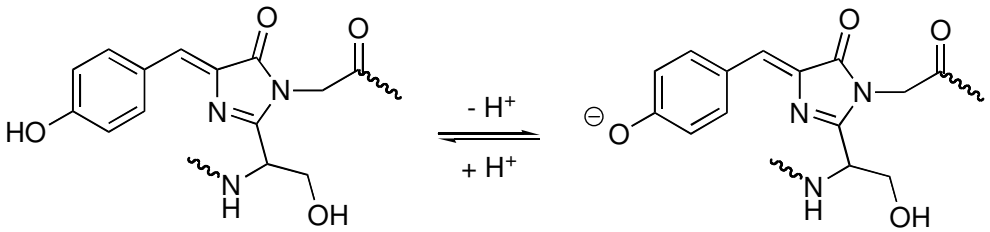

A **B**

SCHEME 3